JOURNAL OF THERMOPHYSICS AND HEAT TRANSFER
Vol. 20, No. 1, January–March 2006

Transient Conjugate Heat-Transfer Model for Circular Tubes Inside a Rectangular Substrate

P. S. C. Rao* and Muhammad M. Rahman†
University of South Florida, Tampa, Florida 33620

The transient heat transfer for laminar flow inside a circular microtube, embedded in a rectangular substrate, during power startup has been numerically investigated using the finite element method. Silicon and silicon carbide were the substrates used, and water and FC-72 were the working fluids. Equations governing the conservation of mass, momentum, and energy were solved in the fluid region. Within the solid wafer, the heat-conduction equation was solved. A thorough investigation for velocity and temperature distributions for different substrates and coolants was performed by varying geometrical dimensions. The Prandtl number, thermal conductivity ratio, and diameter ranges were 6.78–12.68, 27–2658, and 300–1000 μm, respectively. It was determined that a larger diameter tube or a higher thermal conductivity of the substrate material results in a shorter duration of the transient. Nusselt number decreases with time and asymptotically reaches the steady-state condition. It was observed that enlarging the tube from 300 to 1000 μm results in lowering of the fluid mean temperature at the exit. It was also found that a higher Prandtl-number fluid yields higher maximum substrate temperatures and Nusselt numbers.

Nomenclature

B	=	half of tube spacing, m
C_p	=	specific heat, J/kg · K
D	=	tube diameter, m
Fo	=	Fourier number, $\alpha_f t/(D/2)^2$
H	=	height of the substrate, m
k	=	thermal conductivity, W/m · K
L	=	tube length, m
Nu	=	local peripheral average Nusselt number, $(q''_{\text{intf}}D)/[k_{\text{f}}(T_{\text{intf}} - T_{\text{b}})]$
Nu_{avg}	=	average Nusselt number for the entire tube
Nu_θ	=	local Nusselt number
nr	=	number of cells in the radial direction within the tube
nx	=	number of cells in the x direction within the substrate
ny	=	number of cells in the y direction within the substrate
nz	=	number of cells in the z direction
P	=	dimensionless pressure, $(p - p_0)/(\rho v_{\text{in}}{}^2)$
Pr	=	Prandtl number, $\mu C_p/k$
p	=	pressure, N/m^2
Q	=	dimensionless local peripheral average interface heat flux, q''_{intf}/q''_w
q''	=	heat flux, W/m^2
R	=	dimensionless radial coordinate, r/H
Re	=	Reynolds number, $(v_{\text{in}}D)/\nu$
r	=	radial coordinate, m
T	=	temperature, °C
V	=	dimensionless velocity, v/v_{in}
v	=	velocity, m/s
X	=	dimensionless horizontal coordinate, x/H
x	=	horizontal coordinate, m
Y	=	dimensionless vertical coordinate, y/H
y	=	vertical coordinate, m
Z	=	dimensionless axial coordinate, z/H
z	=	axial coordinate, m
α	=	thermal diffusivity, $k/(\rho C_p)$, m^2/s
Δ	=	aspect ratio, D/H
η	=	thermal diffusivity ratio, α_s/α_f
θ	=	angular direction
$\theta_{\max}$	=	maximum angular location from bottom to the top of the tube, 180 deg
λ	=	thermal conductivity ratio, k_s/k_f
ν	=	kinematic viscosity, m^2/s
ξ	=	dimensionless axial coordinate, z/L
ρ	=	density, kg/m^3
τ	=	dimensionless time, $(t v_{\text{in}})/D$
Φ	=	dimensionless temperature, $[(T - T_{\text{in}})k_f]/(q''_w D)$
ψ	=	dimensionless angular coordinate, $\theta/\theta_{\max}$

Subscripts

b	=	bulk
f	=	fluid
in	=	inlet
intf	=	interface
m	=	mean
max	=	maximum
o	=	outlet
r	=	radial direction
s	=	solid
w	=	bottom wall of wafer
z	=	axial direction
θ	=	angular direction

Received 27 July 2004; revision received 22 March 2005; accepted for publication 17 April 2005.

*Graduate Research Assistant, Department of Mechanical Engineering, 4202 E. Fowler Avenue, ENB 118.

†Associate Professor; Department of Mechanical Engineering, 4202 E. Fowler Avenue, ENB 118. Member AIAA.

Introduction

THE advent of microchannels has remarkably changed the outlook of microelectro mechanical systems. Over the past 20 years several successful experimental and numerical investigations have led to exponential growth in this technology. As a matter of fact, the increase in power dissipation of electrical circuits has led to the usage of different geometries, different materials, and different coolants as substrates and working fluids to effectively remove the heat. This paper presents a theoretical analysis of fluid flow and heat-transfer processes in circular microtubes embedded in a rectangular substrate during transient startup of power.

Harms et al.[1] carried out experiments on single-phase forced convection in deep rectangular microchannels. Two configurations were tested, a single channel system and a multiple channel system. The results showed that decreasing the channel width and increasing the channel depth provide better fluid flow and heat-transfer

performance. The experimentally obtained local Nusselt number agreed reasonably well with classical developing channel flow theory.

Quadir et al.[2] used a Galerkin finite element formulation to study the performance of a microchannel heat exchanger. The analysis was compared with available experimental, analytical, and computational results for the same channel geometry and fluid flow conditions. Their method predicted the surface temperature, fluid temperature, and total thermal resistance of the heat sink satisfactorily. The method had an additional advantage of considering the nonuniform heat-flux distribution.

Federov and Viskanta[3] numerically studied steady-state, three-dimensional heat transfer in an asymmetric rectangular channel with laminar fluid flow. Silicon was used as the substrate, and water was the working fluid. A uniform heat flux of 90 W/cm^2 was imposed on one of the channel walls. They pointed out that extremely large temperature gradients occur within the solid walls in the immediate vicinity of the channel inlet, which has a potential for significant thermal stresses and structural failure of the heat sink. Toh et al.[4] investigated three-dimensional fluid flow and heat transfer in a microchannel. The effects of various parameters on the local thermal resistance, liquid mass-flow rate in the microchannels, heat flux through the heat sink, and size of the heat sink were examined. The results obtained were compared with the experimental data collected by Tuckerman.[5]

Ameel et al.[6] developed an analytical solution for laminar gas flow in microtubes with a constant heat-flux boundary condition at the wall. The fluid was assumed to be hydrodynamically developed at the tube entrance. The Nusselt number was determined to decrease with increasing Knudsen number. This effect was attributed to an increase in the temperature discontinuity at the wall with increasing Knudsen number. The entrance length was found to vary with Knudsen number, with an increase in slip flow resulting in a longer entrance length.

Adams et al.[7] investigated turbulent, single-phase, forced convection of water in circular microchannels with diameters of 0.76 and 1.09 mm. The experimental Nusselt numbers were generally higher than those predicted by the Gnielinski[8] correlation. A generalized correlation for the Nusselt number for turbulent, single-phase, forced convection in circular microchannels that accommodated smaller diameter channels was developed. Owhaib and Palm[9] experimentally investigated the heat-transfer characteristics of single-phase, forced convection of R-134a through circular microchannels. The diameters were 1.7, 1.2, and 0.8 mm, and both laminar and turbulent flows ($Re = 10^3$–17×10^3) were studied. For $Re < 5 \times 10^3$, the heat-transfer coefficients were almost identical for all three microtube diameters. The experimental Nusselt numbers agreed with classical correlations (macroscale) for fully developed turbulent flow. They also found that the microscale correlations developed by Wu and Little,[10] Yu et al.,[11] and Adams et al.[7] did not agree with the experimentally obtained data.

Shevade and Rahman[12] performed a transient analysis of fluid flow and heat transfer in a rectangular channel, during the magnetic heating of the substrate. Gadolinium was used as the substrate material, and water was the working fluid. It was determined that the peripheral average heat-transfer coefficient and Nusselt number are large near the channel entrance and decrease as the flow proceeds towards the exit. The results also indicated that as the Reynolds number was increased, the outlet temperature decreased, which increased the average heat-transfer coefficient. Rujano and Rahman[13] investigated transient heat transfer for hydrodynamically and thermally developing laminar flow inside a trapezoidal microchannel heat sink. They conducted a systematic study to understand the effects of channel depth and width, Reynolds number, spacing between channels, and solid-to-fluid thermal conductivity ratio. The results showed that the time required for the heat transfer to reach steady-state condition is longer for a system with a larger channel depth or spacing and a smaller channel width or Reynolds number.

Quadir et al.[14] performed a transient finite element analysis of microchannel heat exchangers in a generalized manner so that microchannel design was not restricted to a particular geometry and/or any specific operating conditions. The heat exchanger dimensions of Tuckerman and Pease[15] were employed, and the analysis used water as the working fluid. The performance of the microchannel was obtained as a function of maximum temperature, which was dependent on several nondimensional parameters, chiefly Biot number, conductivity ratio, length-to-width ratio, and length-to-height ratio. This was essentially done so that one could calculate the total thermal resistance.

Jiang et al.[16] fabricated a microsystem consisting of a heater, microchannels, and temperature sensors. The transient temperature behavior of the device was experimentally studied for a variety of power dissipation levels and forced convection flow rates of deionized water. They determined that the dry device heat-up time constant is longer than the cooldown time constant. It was observed that forced convection results in significantly lower operating temperatures as compared to the dry device.

Karimi and Culham[17] numerically studied transient electro-osmotic pumping in rectangular microchannels. The numerical solutions showed significant influences of channel hydraulic diameter, aspect ratio, and applied voltage on the volumetric flow rates under transient and steady-state conditions. They observed that as the channel hydraulic diameter was increased it took longer for the flow to reach steady state. Brutin et al.[18] performed experiments to determine the friction factor of laminar flow in microtubes using transient and steady-state methods. The measured friction factors were slightly higher as compared to the classical Poiseuille law.

From the literature review, it appears that most past studies performed on circular microchannels were experimental in nature and were mostly restricted to steady-state analysis. The studies focused mainly on comparisons with classical theories. In addition, the number of studies on circular microchannel is very small compared to rectangular or trapezoidal microchannels. By numerical simulations, the present research explores transient fluid flow and heat transfer in circular microtubes in a drilled block of rectangular wafer, a configuration commonly used in the fabrication of microelectronics or biomedical devices. A constant heat flux has been applied to one side of the wafer to simulate heat dissipated by embedded microelectronics. The wafer is modeled by taking into account heat generation in circuit components, conduction within the solid, and convection of heat to the working fluid. Circular microtubes using silicon and silicon carbide as wafer materials are considered in this study. Water and FC-72 are used as working fluids. A detailed study is carried out to explore the effects of channel diameter, solid and fluid properties, and Reynolds number on the transient heat-transfer characteristics within the microtube.

Modeling and Simulation

The physical configuration of the system used in the present investigation is schematically shown in Fig. 1. Because of the symmetry of the adjacent channels and uniform heat flux at the bottom, the analysis is performed by considering a crosssection of the heat sink that contains half the distance between tubes in the horizontal direction. It is assumed that the fluid enters the tube at a uniform velocity and temperature, and hence the effects of inlet and outlet plenums are neglected.

The differential equations were solved using dual coordinate systems. In the solid substrate, a Cartesian coordinate system is used. In the fluid region, a cylindrical coordinate system is used. The applicable differential equations in the cylindrical coordinate system for the conservation of mass, momentum, and energy in the fluid region for incompressible flow are[19]

$$\frac{\partial V_r}{\partial R} + \frac{V_r}{R} + \frac{1}{\pi R}\frac{\partial V_\theta}{\partial \psi} + \frac{\partial V_z}{\partial Z} = 0 \tag{1}$$

$$\frac{1}{\Delta}\frac{\partial V_r}{\partial \tau} + V_r\frac{\partial V_r}{\partial R} + \frac{V_\theta}{\pi R}\frac{\partial V_r}{\partial \psi} - \frac{V_\theta^2}{R} + V_z\frac{\partial V_r}{\partial Z} = -\frac{\partial P}{\partial R} + \frac{\Delta}{Re}\left(\frac{\partial^2 V_r}{\partial R^2} + \frac{1}{R}\frac{\partial V_r}{\partial R} - \frac{V_r}{R^2} + \frac{1}{\pi^2 R^2}\frac{\partial^2 V_r}{\partial \psi^2} - \frac{2}{\pi R^2}\frac{\partial V_\theta}{\partial \psi} + \frac{\partial^2 V_r}{\partial Z^2}\right) \tag{2}$$

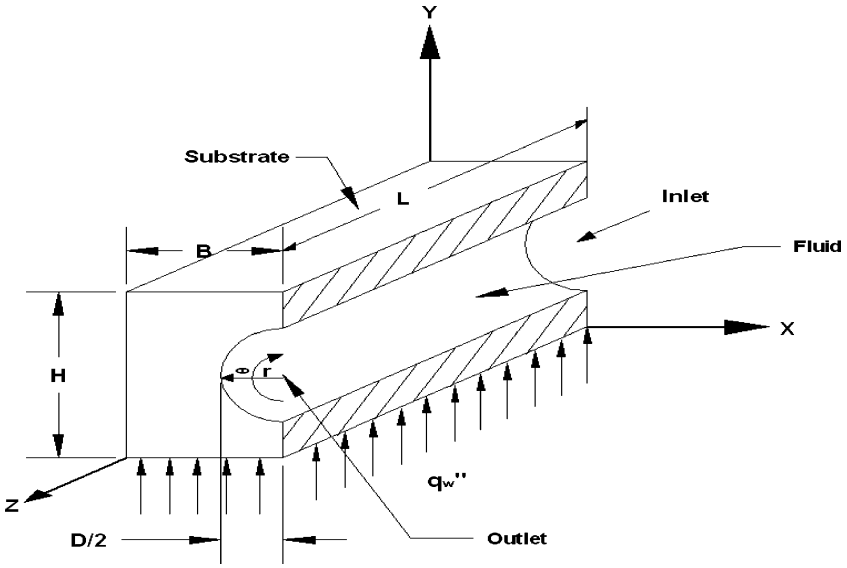

Fig. 1 Three-dimensional view of a section of microtube heat sink.

$$\frac{1}{\Delta}\frac{\partial V_\theta}{\partial \tau} + V_r\frac{\partial V_\theta}{\partial R} + \frac{V_\theta}{\pi R}\frac{\partial V_\theta}{\partial \psi} + \frac{V_r V_\theta}{R} + V_z\frac{\partial V_\theta}{\partial Z} = -\left(\frac{1}{\pi R}\frac{\partial P}{\partial \psi}\right) + \frac{\Delta}{Re}\left(\frac{\partial^2 V_\theta}{\partial R^2} + \frac{1}{R}\frac{\partial V_\theta}{\partial R} - \frac{V_\theta}{R^2} + \frac{1}{\pi^2 R^2}\frac{\partial^2 V_\theta}{\partial \psi^2} + \frac{2}{\pi R^2}\frac{\partial V_r}{\partial \psi} + \frac{\partial^2 V_\theta}{\partial Z^2}\right) \tag{3}$$

$$\frac{1}{\Delta}\frac{\partial V_z}{\partial \tau} + V_r\frac{\partial V_z}{\partial R} + \frac{V_\theta}{\pi R}\frac{\partial V_z}{\partial \psi} + V_z\frac{\partial V_z}{\partial Z} = -\frac{\partial P}{\partial Z} + \frac{\Delta}{Re}\left(\frac{\partial^2 V_z}{\partial R^2} + \frac{1}{R}\frac{\partial V_z}{\partial R} + \frac{1}{\pi^2 R^2}\frac{\partial^2 V_z}{\partial \psi^2} + \frac{\partial^2 V_z}{\partial Z^2}\right) \tag{4}$$

$$\frac{1}{\Delta}\frac{\partial \Phi_f}{\partial \tau} + V_r\frac{\partial \Phi_f}{\partial R} + \frac{V_\theta}{\pi R}\frac{\partial \Phi_f}{\partial \psi} + V_z\frac{\partial \Phi_f}{\partial Z} = \frac{\Delta}{RePr}\left(\frac{\partial^2 \Phi_f}{\partial R^2} + \frac{1}{R}\frac{\partial \Phi_f}{\partial R} + \frac{1}{\pi^2 R^2}\frac{\partial^2 \Phi_f}{\partial \psi^2} + \frac{\partial^2 \Phi_f}{\partial Z^2}\right) \tag{5}$$

For the temperatures considered in this investigation, the variation of fluid properties with temperature is assumed to be negligible. Additionally, viscous dissipation and pressure work, which are commonly encountered in high-speed flow, are expected to be insignificant for the conditions investigated in this work. The equation for heat conduction in the solid region is[20]

$$\frac{\partial \Phi_s}{\partial \tau} = \frac{\eta \Delta^2}{RePr}\left(\frac{\partial^2 \Phi_s}{\partial X^2} + \frac{\partial \Phi_s}{\partial Y^2} + \frac{\partial^2 \Phi_s}{\partial Z^2}\right) \tag{6}$$

The following initial and boundary conditions have been employed:
At $\tau = 0$,

$$\Phi_s = \Phi_f = 0 \tag{7}$$

At $Z = 0, 0 < R < \Delta/2$,

$$V_r = 0, \qquad V_\theta = 0, \qquad V_z = 1, \qquad \Phi_f = 0 \tag{8}$$

At $Z = L/H, 0 < R < \Delta/2$,

$$P = 0, \qquad \frac{\partial V_z}{\partial Z} = 0, \qquad \frac{\partial \Phi_f}{\partial Z} = 0 \tag{9}$$

At $X = B/H, (1-\Delta)/2 < R < (1+\Delta)/2, 0 < Z < L/H$,

$$V_\theta = 0, \qquad \frac{\partial V_r}{\partial X} = 0, \qquad \frac{\partial V_z}{\partial X} = 0, \qquad \frac{\partial \Phi_f}{\partial X} = 0 \tag{10}$$

At $Y = 0, 0 < X < B/H, 0 < Z < L/H$,

$$\frac{\partial \Phi_s}{\partial Y} = -\frac{1}{\Delta\lambda} \tag{11}$$

At $R = \Delta/2, 0 < Z < L/H$,

$$\Phi_s = \Phi_f, \qquad \frac{\partial \Phi_s}{\partial R} = \frac{\partial \Phi_f}{\partial R} \tag{12}$$

The remaining sides of the solid substrate are symmetric or insulated where the temperature gradient normal to the surface is zero.

It can be observed that the nondimensionalization of the governing transport equations and boundary conditions were carried out using the height of the substrate as the length scale and the inlet velocity as the velocity scale. All dimensionless groups are defined in the Nomenclature. The Reynolds number is the most important flow parameter in the governing equations. The transport properties give rise to three important dimensionless groups, namely, Prandtl number Pr, solid-to-fluid thermal conductivity ratio λ, and solid-to-fluid thermal diffusivity ratio η. The important geometrical parameters are L/H, B/H, channel aspect ratio Δ, and the dimensionless axial coordinate ξ. The dimensionless time τ has been defined with D/v_{in} as the timescale. It can be related to Fourier number Fo as $\tau = Fo \cdot Re \cdot Pr$. The dependent variables, selected to specify the results, are the dimensionless temperature Φ, the dimensionless interfacial heat flux Q, and the Nusselt number Nu.

The governing equations along with the initial and boundary conditions Eqs. (7–12) were solved using the Galerkin finite element method. Equations for solid and fluid phases were solved simultaneously as a single-domain conjugate problem. Four-node quadrilateral elements were used. In each element, the velocity, pressure, and temperature fields were approximated, which resulted in a set of equations that defined the continuum. The Newton–Raphson algorithm was used to solve the nonlinear system of discretized equations, and an iterative procedure was used to arrive at the solution for the velocity and temperature fields. The numerical model and the solution algorithm were implemented in the commercial code FIDAP. The solution was considered converged when the field values became approximately constant, and relative changes from one iteration to the next were less than 0.0001%.

The distribution of cells in the computational domain was determined from a series of tests with different numbers of elements in the x, y, and z directions. The results, obtained by using $8 \times 48 \times 40$ (in the radial direction, number of cells, $nr = 24$) and $10 \times 64 \times 40$ ($nr = 32$), captured most of the changes occurring in the system. The dimensionless local peripheral average interface temperature

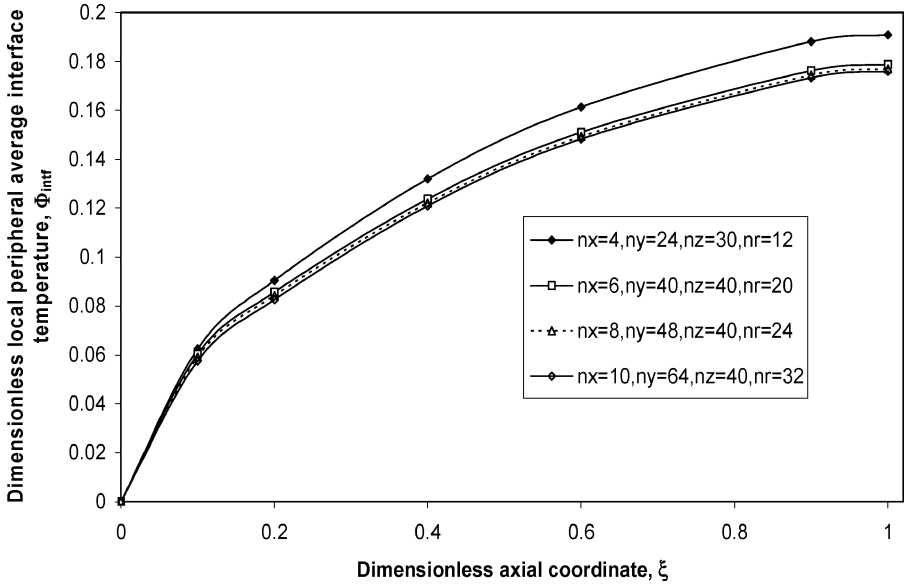

Fig. 2 Variation of dimensionless local peripheral average interface temperature along the length of the tube for different grid sizes (substrate = silicon, coolant = water, $\lambda = 248$, $\Delta = 0.25$, and $Re = 1.5 \times 10^3$).

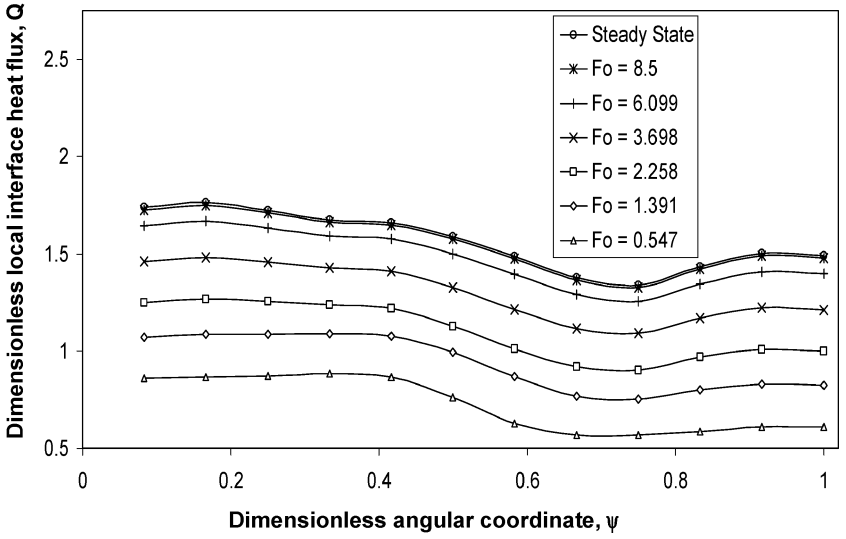

Fig. 3 Variation of dimensionless local interface heat flux around the periphery of the smaller diameter tube at different time intervals (substrate = silicon, coolant = water, $\lambda = 248$, $\Delta = 0.15$, $\xi = 0.4$, and $Re = 1.5 \times 10^3$).

distributions as seen in Fig. 2 were within 0.75% of one another. Therefore, the domain consisting of $8 \times 48 \times 40$ elements in the x-, y-, and z-coordinate directions along with 24 cells in the radial direction (within the tube) was chosen for all numerical computations. The problem was tested for several increments of time, and in each case the distribution of average interface temperature along the tube length was graphed. The time increment of 0.005 s was selected because the resulting temperature distributions when using 0.001-s, 0.005-s, and 0.01-s increments were practically the same.

Results and Discussion

A thorough investigation of velocity and temperature distribution in the microtube is performed by varying the diameter. Silicon (Si) and silicon carbide (SiC) are the substrate materials, and water (W) and FC-72 (FC) are the working fluids. The length of the microtube is kept constant for all of the configurations, namely, 0.025 m. When water is used as the working fluid, a constant heat flux of 300 kW/m^2 is applied to the bottom of the wafer. A constant heat flux measuring 40 kW/m^2 is applied when FC-72 is used. The fluid enters the tube at a uniform velocity and constant inlet temperature $T_{in} = 20^\circ$C. Interfacial temperature, interfacial heat flux, heat-transfer coefficient, and Nusselt number are calculated at different positions along the length of the tube. The configuration is investigated for diameters D 300, 500, 1000 μm and heat flux q'' 40 and 300 kW/m^2. The dimensions in Fig. 1 are $B = 1000$ μm, $H = 2000$ μm, and $L = 0.025$ m. These dimensions are typical for a small size heat exchanger being developed for a compact magnetic refrigerator for space applications. Systems developed for biomedical or sensor applications might have channel sizes smaller than 300 μm. Even though the results are presented in dimensionless form, they should be used only for microtubes or minitubes where a laminar flow can be maintained.

The dimensionless local interfacial heat flux is calculated for different time intervals. Figures 3 and 4 show the variation of dimensionless local interfacial heat flux along the periphery of the tube at different time intervals for the silicon and water combination. The aspect ratios are $\Delta = 0.15$ and 0.5, respectively. The Reynolds number of the flow is 1.5×10^3. These plots have been generated for the $\xi = 0.4$ section of the microtube. It is observed that, at all time intervals, the interface heat flux varies over a significant range and

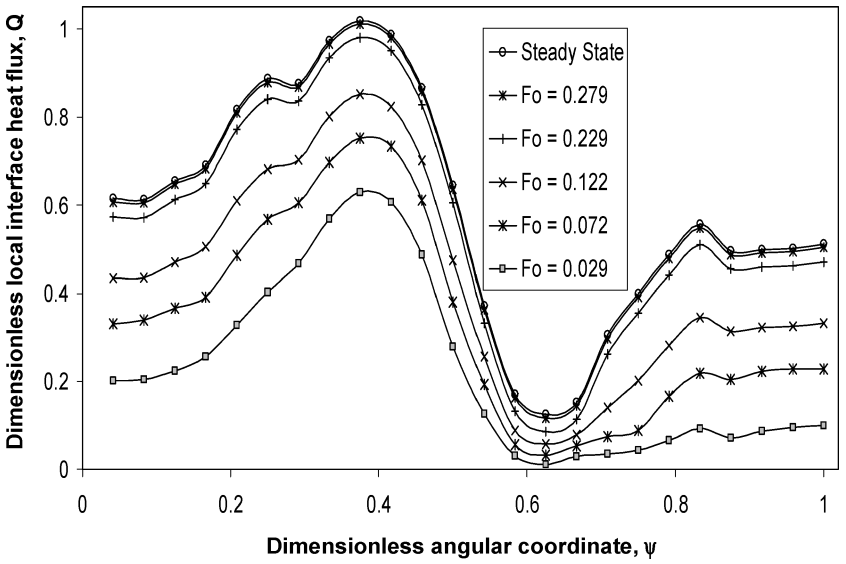

Fig. 4 Variation of dimensionless local interface heat flux around the periphery of the larger diameter tube at different time intervals (substrate = silicon, coolant = water, $\lambda = 248$, $\Delta = 0.5$, $\xi = 0.4$, and $Re = 1.5 \times 10^3$).

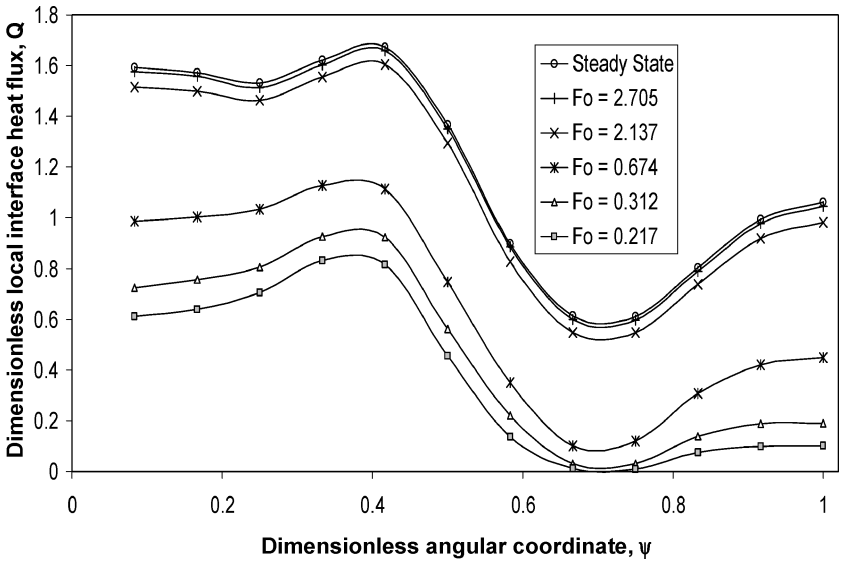

Fig. 5 Variation of dimensionless local interface heat flux around the periphery of the tube at different time intervals (substrate = silicon, coolant = FC-72, $\lambda = 2658$, $\Delta = 0.25$, $\xi = 0.4$, and $Re = 1.5 \times 10^3$).

follows the same distribution pattern from the beginning of the transient to the final steady state. For a smaller aspect ratio ($\Delta = 0.15$), a higher heat flux is seen in the lower portion of the tube and a somewhat lower heat flux in the upper portion of the tube. There is a gradual decrease of heat flux between $\psi = 0.4$ and 0.6. For a larger aspect ratio ($\Delta = 0.5$), the maximum heat flux occurs at approximately $\psi = 0.4$, and there is a steep decrease to the minimum at approximately $\psi = 0.6$. The large variation of heat flux around the tube periphery for this case is believed to be the result of smaller solid volume available for conduction and thermal energy storage that smooth out the temperature distribution at the tube periphery. The maximum apparently happens at a peripheral location in the tube where the average distance to the heated surface is minimum. The minimum heat-flux location approximately corresponds to the minimum distance to the back side of the wafer that is insulated. From the initial time until the heat transfer reaches steady state, the difference between the substrate and fluid temperatures increases. Thus the highest interface heat flux is obtained when the fluid reaches steady state. The fluid flowing in a smaller diameter tube reaches a higher fluid and substrate temperature. The difference between the fluid and substrate temperature for the $\Delta = 0.15$ tube is 10 times that of the $\Delta = 0.5$ tube. Hence, a smaller diameter tube yields a higher interface heat flux. It was found that a smaller diameter tube ($\Delta = 0.15$, $t = 2.35$ s) takes a longer time to reach steady state as compared to a larger tube ($\Delta = 0.5$, $t = 1.94$ s).

Figure 5 shows the variation of dimensionless local interfacial heat flux along the periphery of the tube at different time intervals for a Si–FC ($\lambda = 2658$) combination of the substrate and the coolant. The wafer was analyzed for $\Delta = 0.25$ and $Re = 1.5 \times 10^3$. A graph has been generated for the $\xi = 0.4$ section of the microtube. The plot follows a similar trend as recorded in the preceding cases. The interface heat flux is significantly affected by aspect ratio Δ. In addition, FC-72 has a lower thermal conductivity as compared to water. It was also found that, in the case of same coolant flowing in different substrates, the difference in the interface heat-flux values is not very significant. The SiC–W ($\lambda = 189$) combination attained a higher interface heat flux as compared to the Si–W ($\lambda = 248$), SiC–FC ($\lambda = 2020$), and Si–FC ($\lambda = 2658$) combinations. This can be attributed to the decreasing thermal conductivity ratios of the corresponding combinations. The SiC–FC combination takes longest

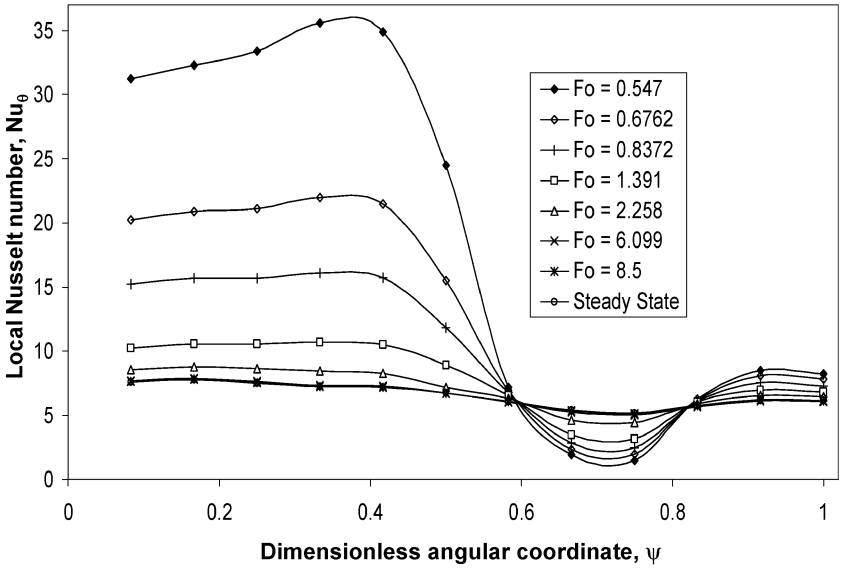

Fig. 6 Variation of local Nusselt number around the periphery of the tube at different time intervals (substrate = silicon, coolant = water, $\lambda = 248$, $\Delta = 0.15$, $\xi = 0.4$, and $Re = 1.5 \times 10^3$).

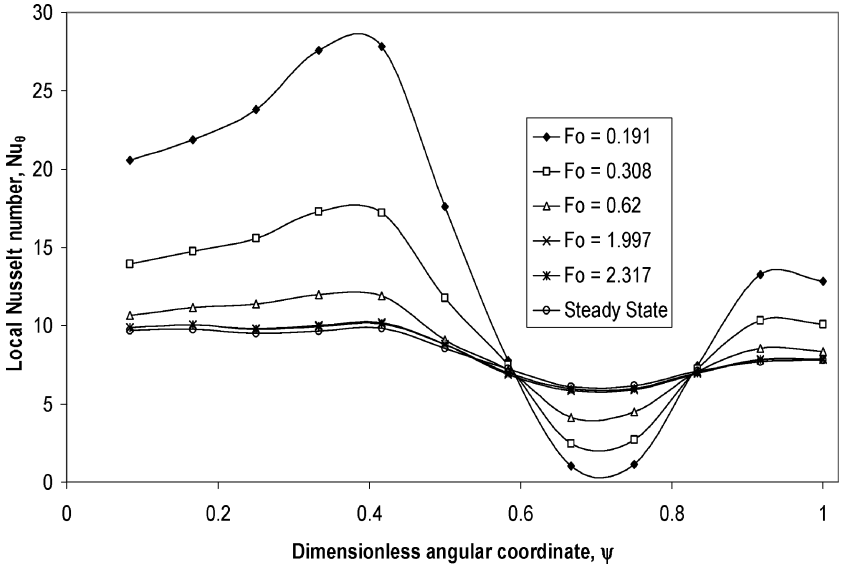

Fig. 7 Variation of local Nusselt number around the periphery of the tube at different time intervals (substrate = silicon, coolant = water, $\lambda = 248$, $\Delta = 0.25$, $\xi = 0.4$, and $Re = 1.5 \times 10^3$).

($t = 10.46$ s) to reach steady state, and the Si–W combination takes the least time ($t = 2.05$ s). The Si–FC combination attains steady state in 8.21s.

Figures 6 and 7 show the variation of local Nusselt number along the periphery of the tube for the silicon and water combination at different time intervals for $\Delta = 0.15$ and 0.25. The local Nusselt number was calculated at $\xi = 0.4$. At all time intervals, as one moves along the periphery of the tube in the θ direction, a sinusoidal variation of the Nusselt number is observed. During the initial stage, a significant variation in the Nusselt number is observed, and as the fluid reaches steady state the values vary over a much smaller range. As time progresses, the temperature of the fluid increases in the θ direction at all sections of the tube, unlike the interfacial heat flux, which continues to vary all around the tube periphery and increases gradually. The rate at which the interfacial heat flux increases along the tube length is slower when compared to the increase in fluid temperature. Thus, as time increases, a decreasing trend in Nusselt number is recorded at all sections of the tube. The lowest average Nusselt number is recorded at steady state. The Nusselt number is higher for $\Delta = 0.25$ as compared to $\Delta = 0.15$. Because the Reynolds number is kept constant, the diameter of the larger tube results in the higher Nusselt number. In addition, a larger diameter, or consequently smaller solid volume between the heater and the fluid, results in larger fluctuation of Nusselt number around the tube periphery during the entire transient process.

Figure 8 shows the local Nusselt-number variation along the periphery of the tube for the Si–FC combination of substrate and working fluid at different time intervals (at $\xi = 0.4$). The wafer was analyzed for $\Delta = 0.25$ and $Re = 1.5 \times 10^3$. The trend in variation of Nusselt number in the θ direction is similar in both cases: same coolant flowing in different substrates and different coolants flowing in a single substrate. In all cases, the Nusselt number starts with a high value and decreases with time. As the flow reaches steady state, the values vary over a much smaller range. In the case of different coolants flowing in the same substrate (Figs. 7 and 8), the Si–FC combination attains higher Nusselt numbers as compared to the Si–W combination. The lower thermal conductivity of FC-72 as compared to water results in higher Nusselt numbers for the

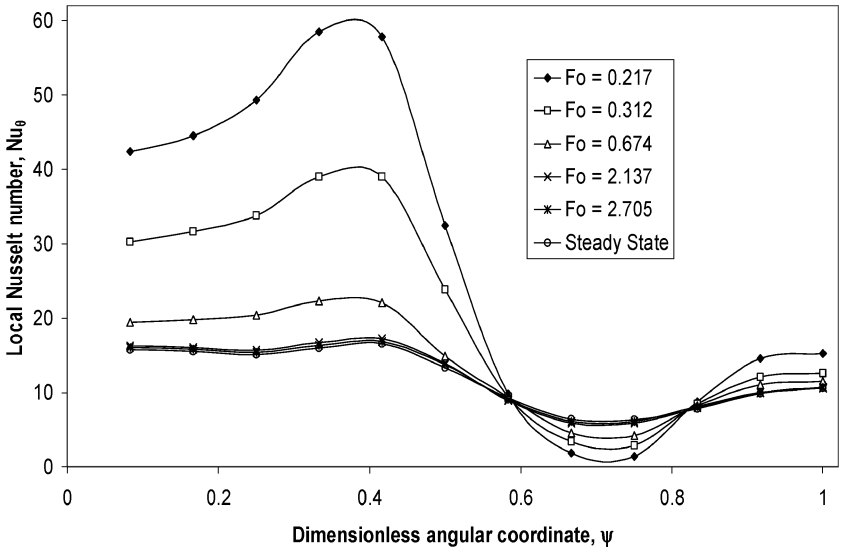

Fig. 8 Variation of local Nusselt number around the periphery of the tube at different time intervals (substrate = silicon, coolant = FC-72, $\lambda = 2658$, $\Delta = 0.25$, $\xi = 0.4$, and $Re = 1.5 \times 10^3$).

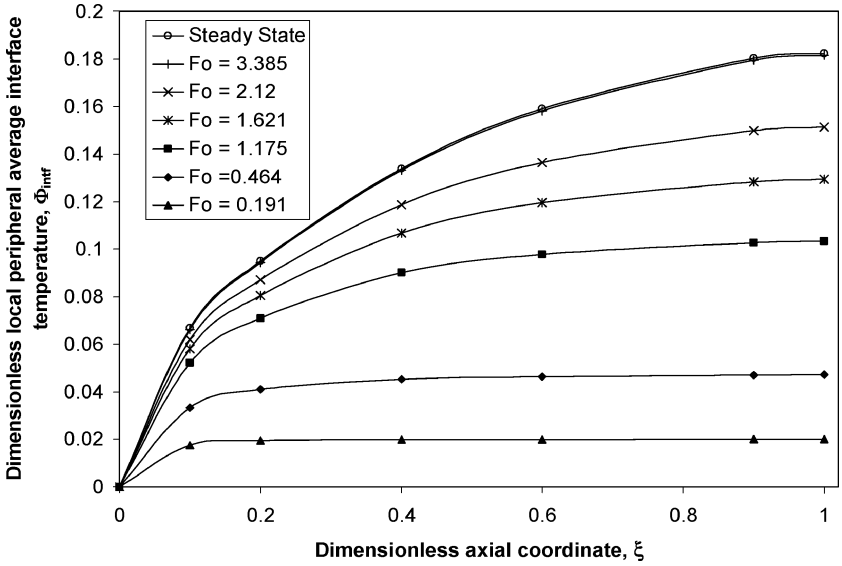

Fig. 9 Variation of dimensionless local peripheral average interface temperature along the length of the tube at different time intervals (substrate = silicon carbide, coolant = water, $\lambda = 189$, $\Delta = 0.25$, and $Re = 1.5 \times 10^3$).

Si–FC combination. The difference in the Nusselt numbers at any given time was not found to be very significant in the case of the same coolant flowing in different substrates. A higher λ value yields higher Nusselt numbers at all sections of the tube and at all times. Thus higher Nusselt numbers are obtained by combinations in the following order: Si–FC > SiC–FC > Si–W > SiC–W.

Figures 9 and 10 show the variation of dimensionless local peripheral average interface temperature along the tube length for SiC–W and SiC–FC combinations at different time intervals. As the fluid enters the tube, it tends to remove heat from the tube wall. In this process, the fluid absorbs heat and exits the tube at a higher temperature. The fluid tends to take heat from the walls at all times. In addition, thermal energy is stored in both the solid and the fluid until steady state is reached. It can be noted that, during the earlier part of the transient, the dimensionless interface temperature increases nearly linearly at large distances from the entrance. During the later part of the transient, the temperature profile shows a larger slope at smaller ξ, and the slope decreases at larger ξ locations. Because of the lower thermal diffusivity of the fluid, the thickness of the thermal boundary layer remains very thin and uniform during the early part of the transient. As Fourier number increases, the boundary layer thickens and approaches the steady characteristics of zero thickness at the leading edge and gradually increasing thickness with distance from the leading edge over the entire length of the developing flow region. For a given substrate, FC-72 attains a lower interface temperature as compared to water. As the thermal capacity and conductivity of water are higher than FC-72, this results in higher interface temperature attainment. When water or FC-72 flowed in different substrates, the variation in interface temperature was not significantly different than that observed in the earlier case.

The SiC–W ($\lambda = 189$) and the Si–FC ($\lambda = 2658$) combinations resulted in the highest and lowest dimensionless interface temperatures, respectively. When FC-72 is used as the working fluid, an order-of-magnitude higher temperature difference is seen at the interface. A much larger heat transfer is realized when water is used as the working fluid, because its thermal conductivity is more than 10 times that of FC-72. As the dimensionless interface temperature is directly proportional to the product of temperature difference and thermal conductivity of the fluid, a substrate with water as the coolant attains higher dimensionless interface temperature.

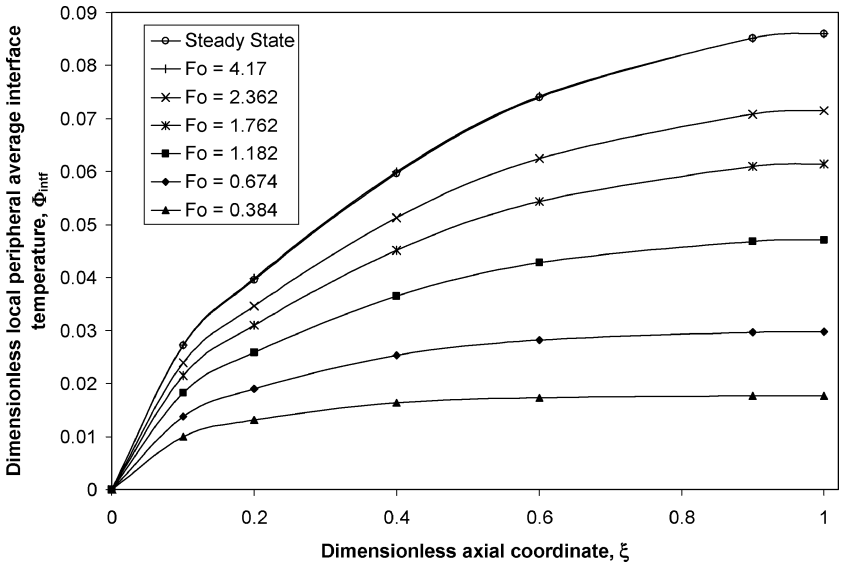

Fig. 10 Variation of dimensionless local peripheral average interface temperature along the length of the tube at different time intervals (substrate = silicon carbide, coolant = FC-72, $\lambda = 2020$, $\Delta = 0.25$, and $Re = 1.5 \times 10^3$).

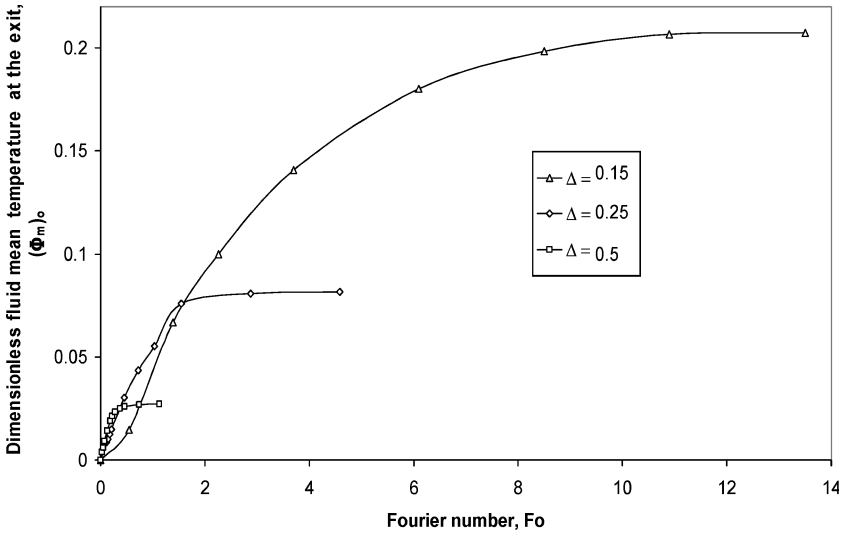

Fig. 11 Variation of dimensionless transient fluid mean temperature at the exit for different inlet diameters (substrate = silicon, coolant = water, $\lambda = 248$, and $Re = 1.5 \times 10^3$).

The effects of solid properties are determined to be much smaller as compared to that of the fluid. It was also observed that, for a constant Reynolds number, a tube with larger Δ yields a lower interface temperature.

The fluid mean temperature at the exit has been used to present the transient response of the substrate and coolant combinations. As the temperature at the inlet remains constant, $(\Phi_m)_o$ essentially represents the total heat-transfer rate in the microtube for any given mass flow rate. Figure 11 shows the variation of dimensionless fluid mean temperature at the exit with Fourier number for different inlet diameters for the silicon and water combination. All of the configurations were analyzed for $Re = 1.5 \times 10^3$. Enlarging the tube from 300 μm ($\Delta = 0.15$) to 1000 μm ($\Delta = 0.5$) leads to a lower mean fluid temperature at the exit. This can be understood by recognizing that the energy storage capacity of the system increases as the diameter is increased, which reduces the fluid temperature, when part of the silicon ($C_p = 715$ J/kg-K) is substituted by water ($C_p = 4179$ J/kg-K) having higher thermal capacity.

Figure 12 shows the variation of dimensionless fluid mean temperature at the exit with Fourier number for four combinations of substrates and coolants. All of the configurations were analyzed for $\Delta = 0.25$ and $Re = 1.5 \times 10^3$. In the case of two different coolants flowing in a single substrate, FC-72's lower thermal conductivity results in a lower dimensionless exit temperature. The specific heat of FC-72 is 25% of that of water. Therefore, for any given heat flux the tube outlet temperature is expected to be higher than water by approximately a factor of four. However, its thermal conductivity is also much lower, only about 9.4% of that of water. Because the fluid thermal conductivity is used in the definition of dimensionless temperature, the outlet temperature in the dimensionless form turns out to be lower for FC-72 as compared to that for water. In the case of the same coolant flowing in two different substrates, a higher λ combination yields a higher dimensionless fluid temperature at the exit. Although the SiC–W and the SiC–FC combinations attain higher fluid temperature at the exit during later part of the transient as compared to the Si–W and the Si–FC combinations, they require more time to reach steady state.

Figures 13–15 show the peripheral average Nusselt-number distribution along the tube length for different tube diameters with the silicon and water combination at different time intervals. The Nusselt number was calculated using peripheral average interface temperature, peripheral average heat flux, and fluid bulk temperature at

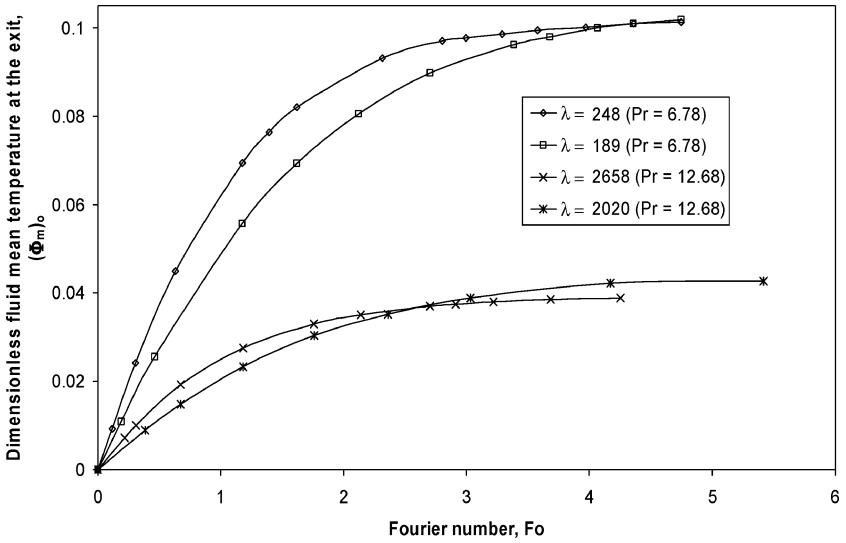

Fig. 12 Variation of dimensionless transient fluid mean temperature at the exit for different combinations of substrates and coolants ($\Delta = 0.25$, and $Re = 1.5 \times 10^3$).

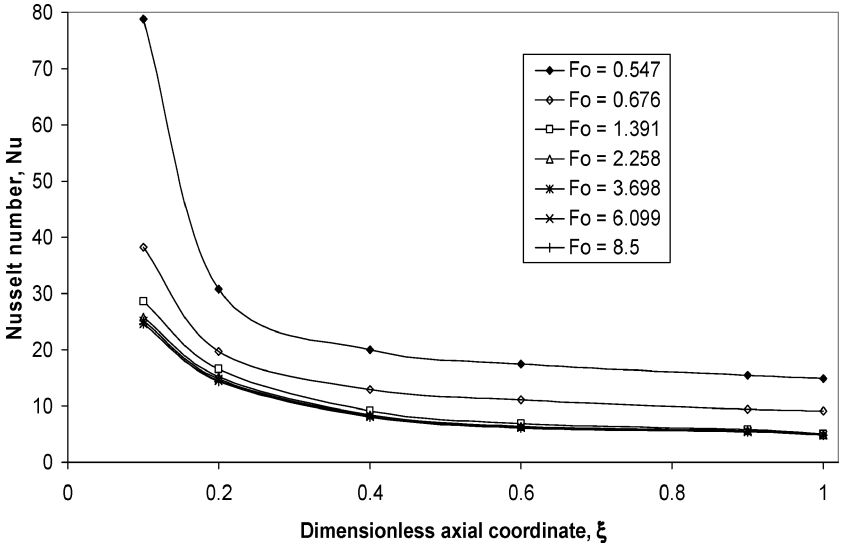

Fig. 13 Variation of Nusselt number along the length of the tube at different time intervals (substrate = silicon, coolant = water, $\lambda = 248$, $\Delta = 0.15$, and $Re = 1.5 \times 10^3$).

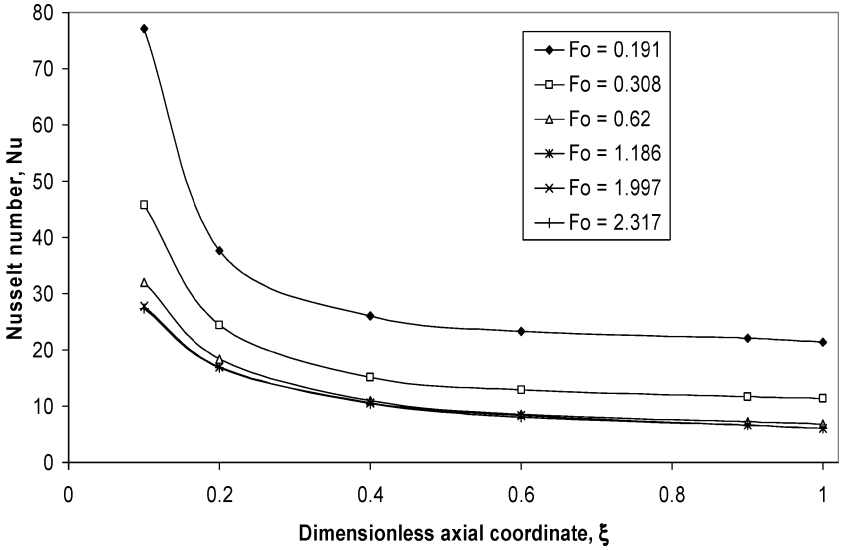

Fig. 14 Variation of Nusselt number along the length of the tube at different time intervals (substrate = silicon, coolant = water, $\lambda = 248$, $\Delta = 0.25$, and $Re = 1.5 \times 10^3$).

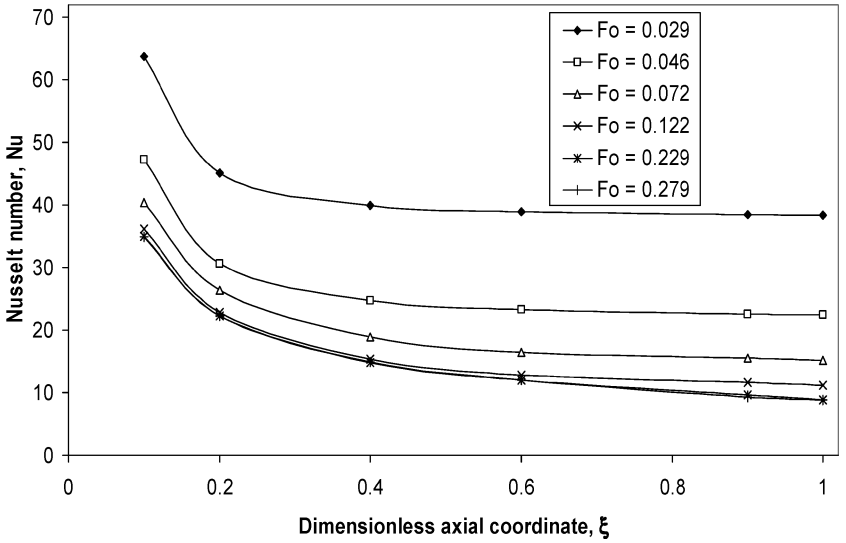

Fig. 15 Variation of Nusselt number along the length of the tube at different time intervals (substrate = silicon, coolant = water, $\lambda = 248$, $\Delta = 0.5$, and $Re = 1.5 \times 10^3$).

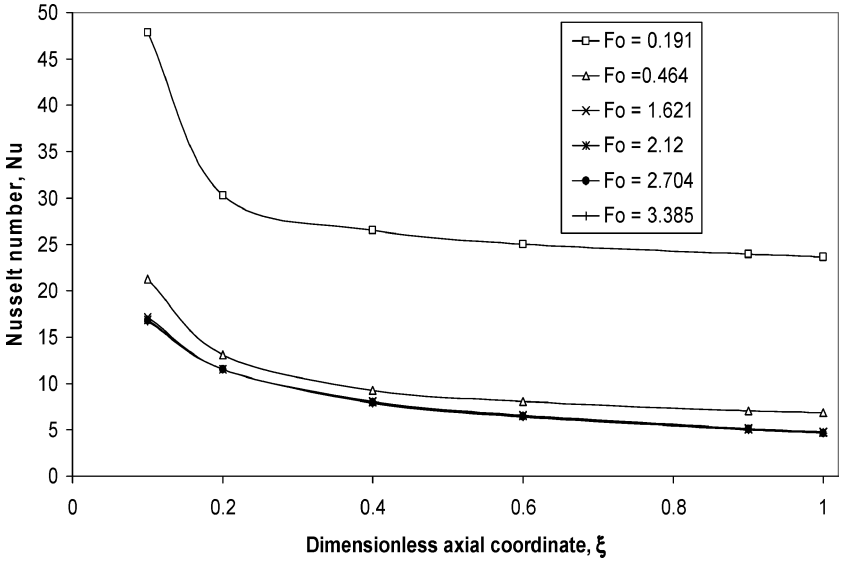

Fig. 16 Variation of Nusselt number along the length of the tube at different time intervals (substrate = silicon carbide, coolant = water, $\lambda = 189$, $\Delta = 0.25$, and $Re = 1.5 \times 10^3$).

that location. Because Fo is calculated using the radius of the tube as the length scale, its value is different in these plots for the same dimensional time. As the fluid flows from the inlet to the outlet, the Nusselt number decreases along the tube length. During the transit, the fluid absorbs heat all along its path. But the amount of heat absorbed decreases all along the tube length. This can be attributed to the development of thermal boundary layer along the tube wall. As the thickness of the boundary layer increases, the resistance to heat transfer from the wall to the fluid increases. As expected, Nusselt number is very high near the entrance and approaches a constant asymptotic value as the flow approaches the fully developed condition. The Nusselt number decreases with time because of the increment of thermal boundary-layer thickness with time as more heat is transmitted from the solid wall to the fluid. As the flow reaches steady state, a very small variation in Nusselt number is recorded. It was also determined that, as the tube diameter is increased, the thermal entrance length becomes longer, which leads to higher Nusselt number. A fully developed condition is approached for smaller diameters whereas for larger diameters the Nusselt number keeps decreasing all of the way to the exit. Therefore, the smaller diameter tube ($\Delta = 0.15$) attains $Nu = 4.33$ and the larger tube ($\Delta = 0.5$) attains $Nu = 9.84$ at steady state. It is also observed that a larger diameter tube results in a better thermal transport as it can carry a larger mass of fluid than a smaller diameter tube for a given Reynolds number.

Figures 16 and 17 show the variation of peripheral average Nusselt number along the length of the tube for the SiC–W and the SiC–FC combinations at different time intervals. It is observed that the trend is similar to the plots in Figs. 13–15. The lower thermal conductivity of FC-72 is the reason for the resulting higher Nusselt numbers. It was observed that a lower λ combination attains fully developed condition and yields a smaller entrance length. In the case of the same coolant flowing in different substrates, no great difference in Nusselt numbers was observed. The SiC–W ($\lambda = 189$) and the Si-FC ($\lambda = 2658$) combinations attain the lowest and the highest Nusselt numbers during the entire transient period, respectively.

Figure 18 shows the variation of average Nusselt number for different inlet diameters for silicon and water combination at different time intervals. It is observed that though smaller diameter tubes take a longer time to reach steady state they do attain the fully developed condition unlike the larger diameter tubes, which take less time and have longer thermal entrance lengths. The average Nusselt number

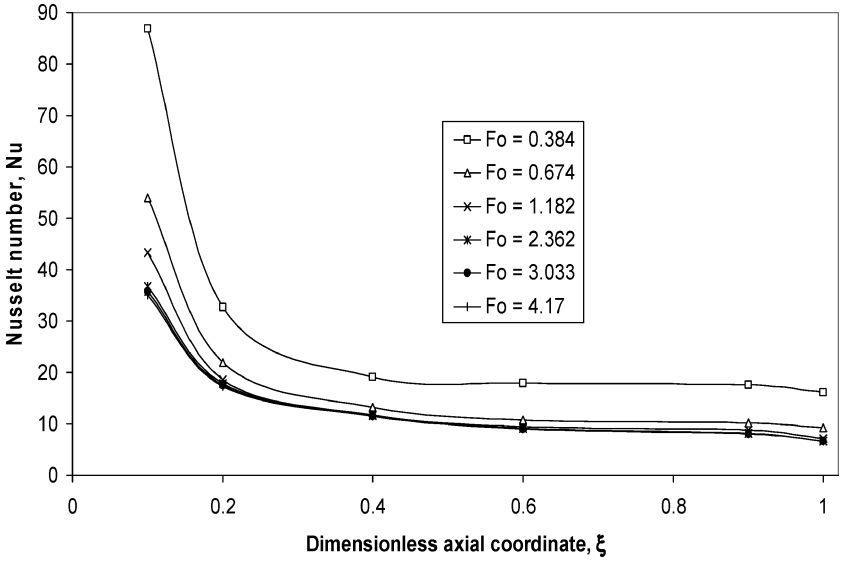

Fig. 17 Variation of Nusselt number along the length of the tube at different time intervals (substrate = silicon carbide, coolant = FC-72, $\lambda = 2020$, $\Delta = 0.25$, and $Re = 1.5 \times 10^3$).

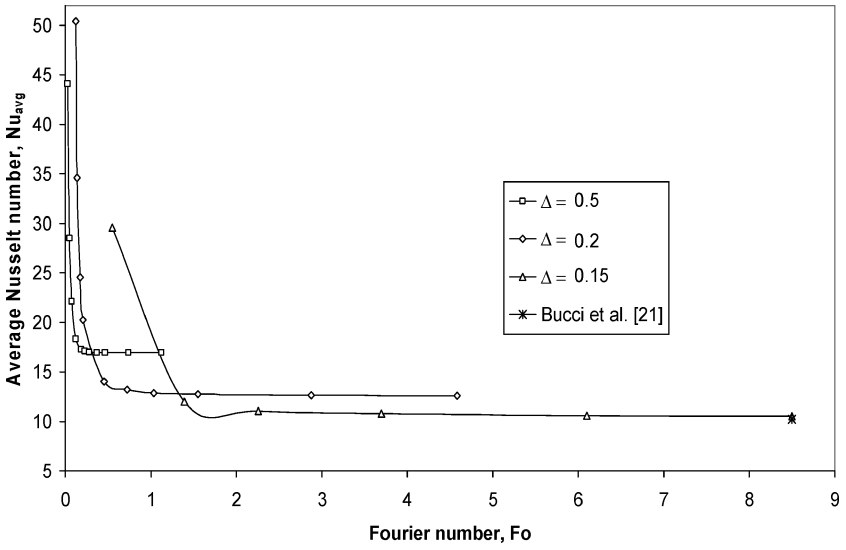

Fig. 18 Transient variation of average Nusselt number for different tube diameters (substrate = silicon, coolant = water, $\lambda = 248$, and $Re = 1.5 \times 10^3$).

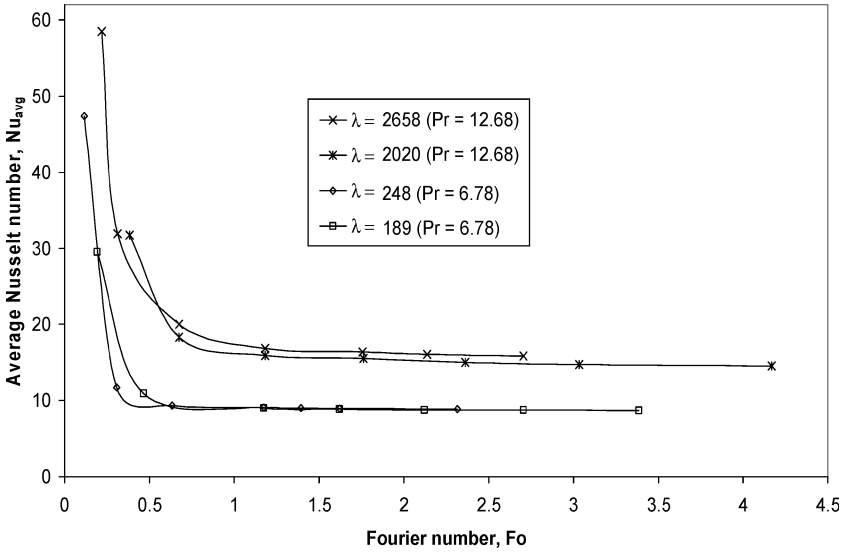

Fig. 19 Transient variation of average Nusselt number for different combinations of substrates and coolants ($\Delta = 0.25$, and $Re = 1.5 \times 10^3$).

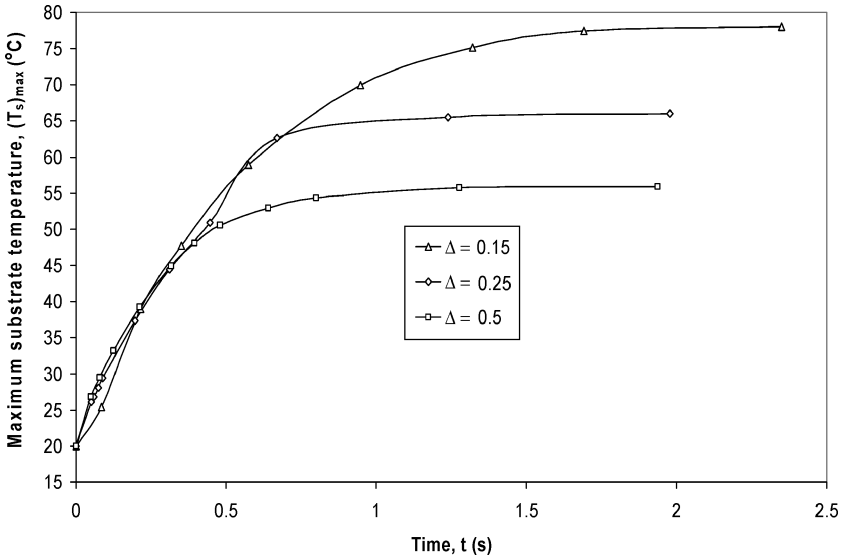

Fig. 20 Transient variation of maximum substrate temperature for different tube diameters (substrate = silicon, coolant = water, $\lambda = 248$, and $Re = 1.5 \times 10^3$).

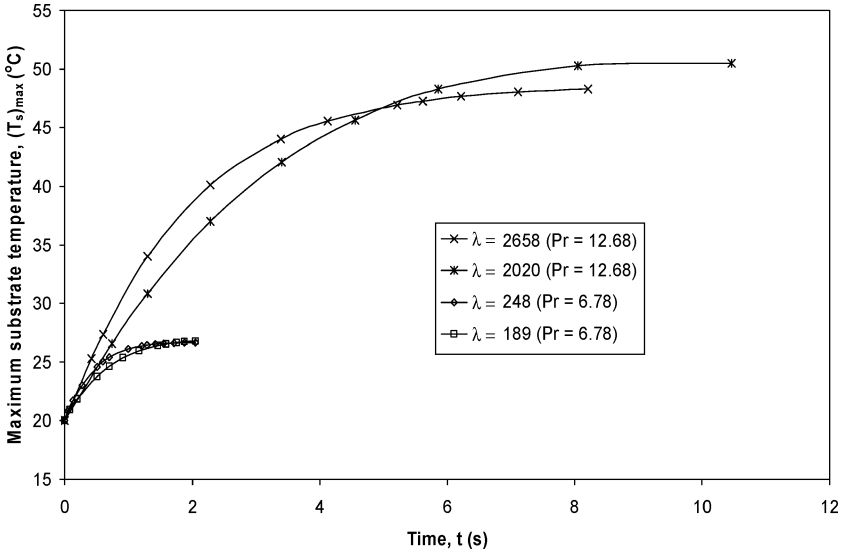

Fig. 21 Transient variation of maximum substrate temperature for different combinations of substrates and coolants ($\Delta = 0.25$, and $Re = 1.5 \times 10^3$).

decreases rapidly in the earlier part of the transient and only gradually as the heat transfer approaches steady state. The figure also makes a comparison with experimentally obtained Nusselt numbers by Bucci et al.,[21] in which they conducted a steady-state analysis of flow inside a 290-μm microtube. Stainless steel was the substrate, and water was the coolant. The numerically obtained Nusselt number is in reasonably good agreement with the experimentally obtained one. The difference is within 3.1%.

Figure 19 shows the variation of average Nusselt number at different time intervals for four combinations of substrates and coolants. It is observed from the figure that higher Prandtl-number fluids attain higher Nusselt numbers. It can also be seen that for a given Prandtl number a lower value of λ results in less time to reach steady state.

Figure 20 shows the variation of maximum substrate temperature for different inlet diameters for the silicon and water combination at different time intervals. The trend is very similar to the one in Fig. 11. The maximum temperature occurs on the plane adjacent to the heater. The fluid flowing in a smaller diameter tube attains a higher maximum substrate temperature as compared to larger diameter tubes because a bigger diameter tube has larger volume of fluid (against the volume of the substrate) to remove heat from the substrate. The magnitude of this substrate temperature is important for the design of cooling systems for microelectronics.

Figure 21 shows the variation of maximum substrate temperature at different time intervals for four combinations of substrates and coolants. It is observed that a higher Prandtl number fluid yields a higher maximum substrate temperature. It is also observed that there is a large variation in the maximum substrate temperature for different fluids flowing in the same substrate. Therefore, the selection of the coolant is very important for the design of thermal management systems. For a given coolant, Si provides a higher maximum temperature in the earlier part of the transient, but a lower maximum temperature in the later part of the transient as compared to SiC. This is because of the difference in thermal storage capacity of the two materials. The magnitude for ρC_p is 1654.3 kJ/m^3-K for Si, whereas 2259.4 kJ/m^3-K for SiC.

Conclusions

The numerical investigation for transient conjugate heat transfer in microtubes was performed by varying the geometric dimensions for different combinations of substrates and working fluids. The distributions of local dimensionless interfacial heat flux and local

Nusselt number around the tube were calculated at different time intervals. For a constant Reynolds number, a tube with a larger diameter attains a lower interface temperature. The Nusselt number is larger near the entrance because of the development of the thermal boundary layer, and it asymptotically approaches a constant value as the flow reaches fully developed condition downstream in the tube. For a constant Reynolds number, the following specific conclusions can be made:

1) A larger aspect ratio Δ tube requires less time to reach steady state.

2) During the earlier part of the transient, the dimensionless interface temperature increases almost uniformly along the entire length of the tube; during the later part of the transient, the temperature increases are larger at larger ξ locations.

3) The dimensionless interface heat flux increases with time and is maximum at steady state.

4) At all locations, Nusselt number decreases with time and approaches the minimum at steady state.

5) Increasing the tube diameter from 300 μm ($\Delta = 0.15$) to 1000 μm ($\Delta = 0.5$) results in lowering of the fluid mean temperature at the exit and increasing the Nusselt number.

6) A higher Prandtl number fluid yields a higher maximum substrate temperature as well as a higher Nusselt number.

Acknowledgments

The authors would like to acknowledge financial support received from NASA under Grant Number NAS3-2751. They would also like to thank Ronald Dougherty and Frank Pyrtle, III, for their helpful suggestions in preparing the final manuscript.

References

[1]Harms, T. M., Kazmierczak, M., and Gerner, F. M., "Developing Convective Heat Transfer in Deep Rectangular Microchannels," *International Journal of Heat and Fluid Flow*, Vol. 20, No. 2, 1999, pp. 149–157.

[2]Quadir, G. A., Mydin, A., and Seetharamu, K. N., "Analysis of Microchannel Heat Exchangers Using FEM," *International Journal of Numerical Methods for Heat and Fluid Flow*, Vol. 11, No. 1, 2001, pp. 59–75.

[3]Fedorov, A. G., and Viskanta, R., "Three-Dimensional Conjugate Heat Transfer in the Microchannel Heat Sink for Electronic Packaging," *International Journal of Heat and Mass Transfer*, Vol. 43, No. 3, 2000, pp. 399–415.

[4]Toh, K. C., Chen, X. Y., and Chai, J. C., "Numerical Computation of Fluid Flow and Heat Transfer in Microchannels," *International Journal of Heat and Mass Transfer*, Vol. 45, No. 26, 2002, pp. 5133–5141.

[5]Tuckerman, D. B., "Heat Transfer Microstructures for Integrated Circuits," Ph.D. Dissertation, Dept. of Electrical Engineering, Stanford Univ., Stanford, CA, 1984.

[6]Ameel, T. A., Wang, X., Barron, R. F., and Warrington, R. O., "Laminar Forced Convection in a Circular Tube with Constant Heat Flux and Slip Flow," *Microscale Thermophysical Engineering*, Vol. 1, No. 4, 1997, pp. 303–320.

[7]Adams, T. M., Abdel-Khalik, S. I., Jeter, S. M., and Qureshi, Z. H., "An Experimental Investigation of Single-Phase Forced Convection in Microchannels," *International Chemical Engineering*, Vol. 41, Nos. 6–7, 1998, pp. 851–857.

[8]Gnielinski, V., "New Equations for Heat and Mass Transfer in Turbulent Pipe and Channel Flow," *International Chemical Engineering*, Vol. 16, No. 2, 1976, pp. 359–368.

[9]Owhaib, W., and Palm, B., "Experimental Investigation of Single-Phase Convective Heat Transfer in Circular Microchannels," *Experimental Thermal and Fluid Science*, Vol. 28, No. 2–3, 2004, pp. 105–110.

[10]Wu, P. Y., and Little, W. A., "Measuring of the Heat Transfer Characteristics of Gas Flow in Fine Channel Heat Exchangers for Micro Miniature Refrigerators," *Cryogenics*, Vol. 24, No. 8, 1984, pp. 415–420.

[11]Yu, D., Warrington, R., Barron, R., and Ameel, T., "An Experimental and Theoretical Investigation of Fluid Flow and Heat Transfer in Microtubes," *Proceedings of the 4th ASME/JSME Thermal Engineering Joint Conference*, Vol. 1, American Society of Mechanical Engineers, New York, 1995, pp. 523–530.

[12]Shevade, S. S., and Rahman, M. M., "Transient Analysis of Microchannel Heat Transfer with Volumetric Heat Generation in the Substrate," *Proceedings of the 2004 TMS Annual Meeting*, The Minerals, Metals, and Materials Society, Warrendale, PA, 2004, pp. 367–380.

[13]Rujano, J. R., and Rahman, M. M., "Transient Response of Microchannel Heat Sinks in a Silicon Wafer," *Journal of Electronic Packaging*, Vol. 119, No. 4, 1997, pp. 239–246.

[14]Quadir, G. A., Beh, S. L., Seetharamu, K. N., and Hassan, A. Y., "A Transient Finite Element Analysis of Microchannel Heat Exchangers," *International Journal of Heat Exchangers*, Vol. 3, No. 1, 2002, pp. 67–88.

[15]Tuckerman, D. B., and Pease, R. F. W., "High Performance Heat Sink for VLSI," *IEEE Electron Device Letters*, Vol. 2, No. 4, 1981, pp. 126–129.

[16]Jiang, L., Wong, M., and Zohar, Y., "Unsteady Characteristics of a Thermal Microsystem," *Sensors and Actuators*, Vol. 82, No. 1–3, 2000, pp. 108–113.

[17]Karimi, G., and Culham, J. R., "Transient Electro-Osmotic Pumping in Rectangular Microchannels," *Proceedings of the International Conference on MEMS, NANO, and Smart Systems*, Inst. of Electrical and Electronics Engineers, IEEE Publications, Piscataway, NJ, 2003, pp. 364–372.

[18]Brutin, D., Topin, F., and Tadrist, L., "Transient Method for the Liquid Laminar Flow Friction Factor in Microtubes," *AIChE Journal*, Vol. 49, No. 11, 2003, pp. 2759–2767.

[19]Bejan, A., *Convection Heat Transfer*, 2nd ed., Wiley, New York, 1994, Chaps. 1 and 3.

[20]Ozisik, M. N., *Heat Conduction*, 2nd ed., Wiley, New York, 1993, p. 67.

[21]Bucci, A., Celata, G. P., Cumo, M., Serra, E., and Zummo, G., "Water Single-Phase Fluid Flow and Heat Transfer in Capillary Tubes," *Proceedings of the 1st International Conference on Microchannels and Minichannels*, American Society of Mechanical Engineers, New York, 2003, pp. 1–8.